Galaxy evolution in different environments along redshift within the local universe $z < 0.8$

Ponlawat Yoifoi[1,2,*] **and Wichean Kriwattanawong**[1]

[1] Department of Physics and Materials Science, Faculty of Science, Chiang Mai University, Chiang Mai, 50200, Thailand

[2] Graduate School, Chiang Mai University, Chiang Mai, 50200, Thailand

*E-mail: ponlawat_yoifoi@cmu.ac.th

Abstract. This study presents the evolution of the galaxies in different matter density along redshift within the local universe. A sample of 702,352 galaxies was collected from the Sloan Digital Sky Survey (SDSS). Under the limitation of the spectroscopic data, the appropriate photometric redshift was used to represent the spectroscopic redshift in the range of $0.0 \leq z \leq 0.8$. Number density of galaxies, galaxy's colors, and star formation activities are considered to describe the evolution of galaxies. In summary, the number density is not clearly different although the Dec and RA of the sky areas are disparate, but it steeply declines along the redshift direction. Considering the number density together with galaxies' Hα emission line from spectroscopic data, we find that both equivalent of hydrogen alpha and Hα flux tend to decrease along the redshift, similar to the decreasing trend of the number density. Furthermore, the galaxy color trend is found to be redder as a function of the redshift for the magnitude range of -19 $\leq M_g \leq$ -17. It implies that the overview of the star formation activity of the fainter galaxies at the lower redshift tend to show higher than the ones at higher redshift.

1. Introduction

Many sky surveys have observed galaxies in several sky regions, depending on the objective of the mission (e.g., The APM galaxy survey [1] and The 2dF Galaxy survey [2]). The APM survey found that the distribution of galaxies showed the presence of some structures connected together in the southern sky area. However, the distribution in the two-dimensional map cannot indicate the entire structure with the combinations of galaxy groups or clusters. Therefore, the three-dimensional galaxy distribution in the 2dF redshift survey is more reasonable way to clearly present the connected structures in the universe. The survey shows that some sky areas are crowded by the numerous galaxies alternating with empty space. For the locations with dense environment in the local universe, galaxy-galaxy and galaxy-cluster interactions can induce star formation activity in the galaxies. The star formation can be traced by Hα emission measurements and corresponding directly to the galaxy color indices [3]. This work aims to study the dependence of star formation activity on the locations having different matter density along the redshift, mainly using the data from the Sloan Digital Sky Survey (SDSS). Sample selection is described in section 2. Section 3 explains the Hα emission and galaxy color analysis. Finally, section 4 contains conclusions of the main results.

2. Sample selection

The SDSS is a large survey, that observed astronomical objects, covering one-third of the entire sky, mostly in the northern galactic and some parts of southern galactic hemisphere. In this work, we collected photometric data from the SDSS Data Released 15 (DR15). In addition, we used spectroscopic data from the Max Planck Institute for Astrophysics and the Johns Hopkins University (MPA-JHU) that measured the galaxies' emission lines, using spectroscopic data in the SDSS Data Released 7 (DR7) [4]. The difference between the two DRs is the observed sky area. For the SDSS DR7, the survey covers the sky areas, RA from $8^{\rm h}$ to $16^{\rm h}$ and declination (δ) from 0° to 70°. While the SDSS DR15 covers the observed sky areas of all previous versions and additional parts in southern galactic sky. Therefore, our sample data are limited by the sky areas of the observations in SDSS DR7. We selected the two sample areas as shown in table 1. However, the spectroscopic redshift data from each selected area are only ∼6000 galaxies. In order to increase more statistical results, it is necessarily to use photometric redshift for the sample galaxies that have no available spectroscopic redshift. Thus, we need to find the variability of the photometric redshift comparing with the accurate spectroscopic redshift data. The standard error of the difference between photometric and spectroscopic redshift was calculated and plotted in figure 1. It is clearly seen that the photometric redshift can appropriately represent the spectroscopic redshift in the range of $z < 0.8$. As a consequence, the galaxies, which have the photometric redshift $z_{photo} < 0.8$, will be counted as our sample. Therefore, we obtained 702,352 sample galaxies, that can provide much better statistical results than the sample used only spectroscopic redshift.

Table 1. The selected sky areas that used in this research.

No.	Centered position with 1° width	
	α	δ
1	10h00m00s (149.5° - 150.5°)	0° - 23° (-0.5° - 23.5°)
2	14h00m00s (209.5° - 210.5°)	0° - 23° (-0.5° - 23.5°)

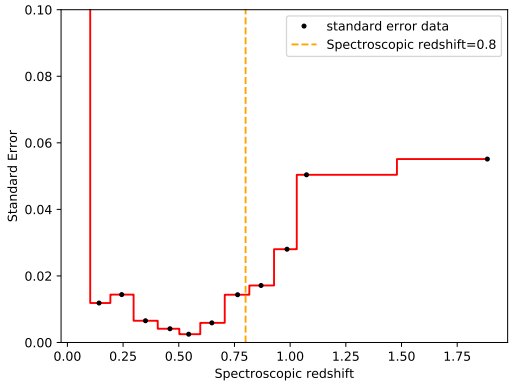

Figure 1. The standard error of the difference between photometric and spectroscopic redshift. The *orange dashed* line shows the selected redshift limit.

The SDSS data were corrected for the Galactic extinction but not for the K-correction. Thus, The K-correction model [5,6] was applied to correct photometric magnitudes for our sample. The sample was subdivided into 48 parts of sky areas with 1×1 $\rm deg^2$. Besides, the sample was subdivided into 13 redshift intervals with a fixed distance of 180 Mpc. In this work, we applied the Hubble constant $H_0 = 67.66$ km $\rm s^{-1}$ $\rm Mpc^{-1}$ [7] to calculate the distance of the sample

galaxies. As a result, we have 624 subsamples, which are statistically sufficient to compare the variation of galaxy parameters distributed in different matter density within $z < 0.8$.

3. Results and discussions

3.1. Number density

The number densities of 624 subsamples were calculated for each volume of a three-dimensional spherical sector [8]. The number densities in some sky areas are plotted against the redshift, as shown in figure 2. The number density in other sky areas show a similar trend as shown in figure-2. The trends of number density gradually drop as a function of redshift in both RA directions. However, there is a "bump" near the redshift z ∼0.4 for all subsamples. With considering the number densities together with the spatial distribution of galaxies in figure 3, they are clearly seen that the number of galaxies is densely populated near the redshift ∼0.4 and lightly for higher redshift.

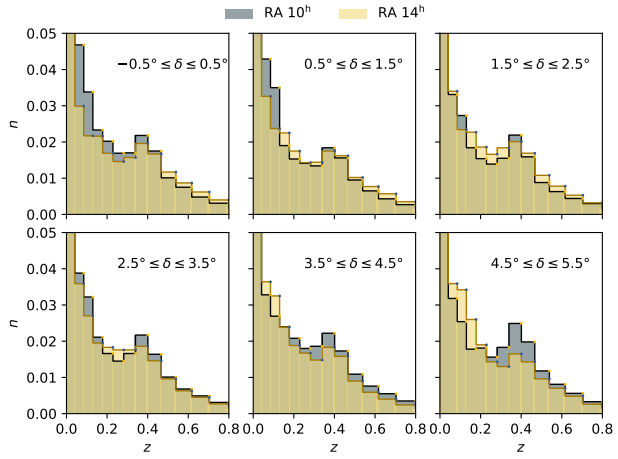

Figure 2. The number density against the redshift bin for both RAs with the declination range from -0.5° to 5.5°.

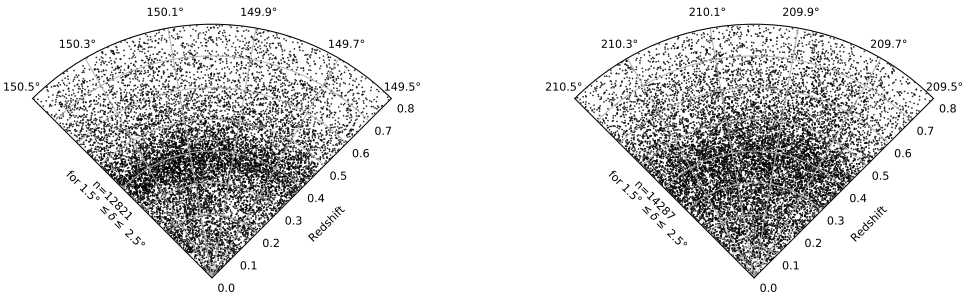

Figure 3. The spatial distribution of sample galaxies in some 1°×1° sky areas for both RAs.

3.2. The Hα emission

The galaxies' emission line from the MPA-JHU spectroscopic data, used in this work, is Hα line. This emission line is typically used to study the star formation activity in the galaxy (e.g., [3,9]). The two important parameters of the Hα emission in this work are the equivalent width of hydrogen alpha ($EW(\mathrm{H}\alpha)$) and Hα flux density. However, the available MPA-JHU data for the Hα line of our sample are only ∼5000 galaxies, i.e., 0.7% of the photometric data. As a consequence, we combined subsamples in all sky areas together for each redshift bin. The average

$EW(\mathrm{H}\alpha)$ and average Hα flux density were then calculated to find the mean characteristic along the redshift. Figures 4 and 5 clearly show that both Hα parameters tend to decrease as a function of redshift. These decreasing trends imply that the star formation activity of galaxies increases toward the very low redshift. Furthermore, there are high fluctuations in both Hα emission densities at the redshift more than 0.3. However, these variations are considered to be negligible when comparing with the values at the very low redshift.

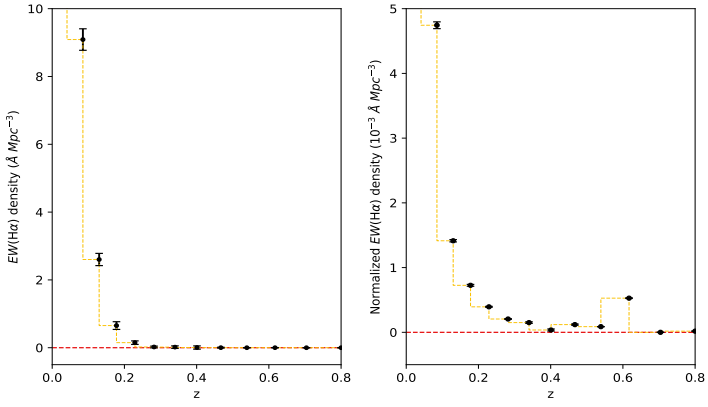

Figure 4. The $EW(\mathrm{H}\alpha)$ density along the redshift. *Left:* The average $EW(\mathrm{H}\alpha)$ density *Right:* The normalised $EW(\mathrm{H}\alpha)$ density by the number of galaxies in those redshift bins.

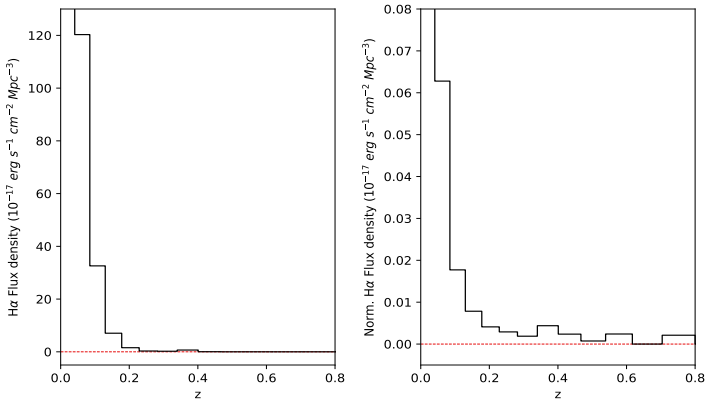

Figure 5. The Hα flux density along the redshift. *Left:* The average Hα flux density *Right:* The normalised Hα flux density by the number of galaxies in those redshift bins.

3.3. The galaxy's color

The color of galaxy is a parameter, widely used to study the stellar content in the galaxy [10]. The three color indices $g-r$, $g-i$, and $r-i$, were calculated and plotted against the redshift, as shown in figures 6 and 7. The M_g band absolute magnitude of the sample is in the range of $-21 \leq M_g \leq -17$. For both RAs, the $g-i$ and $r-i$ colors show upward trends for fainter sample (-19 $\leq M_g \leq$ -17). While a trend of the $g-r$ color trend is nearly constant along the redshift, similar to the trends of the three color indices for the brighter sample (-21 $\leq M_g \leq$ -19). This means that the fainter sample galaxies tend to be bluer as we look toward the lower redshift, consistent to the higher star formation activity at the lower redshift as mentioned above.

4. Conclusions

In this work, the SDSS DR15 and the Hα emission data from the MPA-JHU project were analyzed to investigate the evolution of galaxy parameters within redshift $z \sim 0.8$. Four selected parameters, which are the number density, $EW(\mathrm{H}\alpha)$, Hα flux density, and the color index, were considered to indicate the difference between the two sky areas and along the redshift. The photometric results imply that there exist different matter densities along the redshift. It is

clear that Hα emission and the number density show the decreasing trends as a function of redshift. While the $g-i$ and $r-i$ color indices seem to be redder along the redshift for the fainter galaxies (-19 $\leq M_g \leq$ -17). The results show that the fainter sample galaxies at lower redshift tend to have higher star formation activity than the ones at higher redshift.

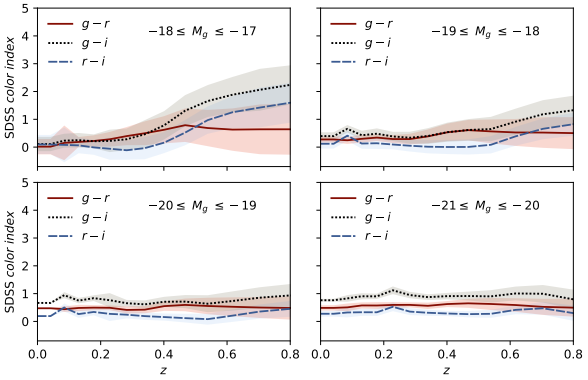

Figure 6. The evolution of average SDSS colors along the redshift at RA $10^{\rm h}$ for each M_g magnitude bin from -21 to -17. *Shaded region:* 1-σ range of uncertainty in SDSS colors.

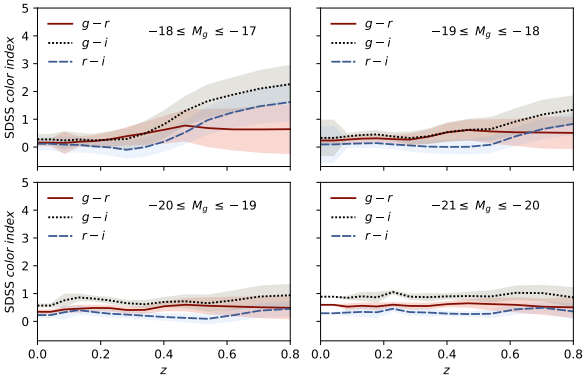

Figure 7. The evolution of average SDSS colors along the redshift at RA $14^{\rm h}$ for each M_g magnitude bin from -21 to -17. *Shaded region:* 1-σ range of uncertainty in SDSS colors.

Acknowledgments

This work has made use of the database of the SDSS. Funding for the SDSS IV has been provided by the Alfred P. Sloan Foundation, the U.S. Department of Energy Office of Science, and the Participating Institutions. The anonymous reviewers are thanked for many helpful comments regarding the content and presentation of this paper.

References

[1] Dalton G B, Maddox S J, Sutherland W J and Efstathiou G 1997 *Mon. Not. R. Astron. Soc.* **289** 263
[2] Peacock J A *et al* 2001 *Nature* **410** 169
[3] Kennicutt Jr R C 1983 *Astrophys. J.* **272** 54
[4] Brinchmann J, Charlot S, White S D M, Tremonti C, Kauffmann G, Heckman T and Brinkmann J 2004 *Mon. Not. R. Astron. Soc.* **351** 1151
[5] Chilingarian I V, Melchior A L and Zolotukhin I Y 2010 *Mon. Not. R. Astron. Soc.* **405** 1409
[6] Chilingarian I V and Zolotukhin I Y 2012 *Mon. Not. R. Astron. Soc.* **419** 1727
[7] Planck Collaboration *et al* 2020 *Astron. Astrophys.* **641** A6
[8] Ly C *et al* 2011 *Astrophys. J.* **726** 109
[9] Kriwattanawong W, Moss C, James P A and Carter D 2011 *Astron. Astrophys.* **527** A101
[10] Baldry I K *et al* 2004 *Astrophys. J.* **600** 681